Vol. **1**, **7**. 513-526 (2005)

Revue de Mécanique Appliquée et Théorique

Modeling of coupled conduction, convection and radiation heat transfers in two-dimensional honeycomb structures

A. Abdelbaki
Departement of Physics, Faculty of Sciences Semlalia, BP. 2390
Marrakech, Maroc.

Z. Zrikem
Departement of Physics, Faculty of Sciences Semlalia, BP. 2390
Marrakech, Maroc.

Résumé
L'objectif du présent travail est d'étudier numériquement le couplage entre les transferts de chaleur par conduction, convection naturelle et rayonnement dans des structures alvéolaires bidimensionnelles. L'application est faite sur les murs alvéolaires des bâtiments construits par des briques creuses en terre cuite à trois ou à quatre rangées verticales d'alvéoles. Les surfaces verticales des structures étudiées sont supposées isothermes et celles horizontales sont adiabatiques ou obéissantes à une condition de périodicité. Les équations de conservation de la masse, de la quantité de mouvement et de l'énergie sont discrétisées par la méthode des volume de contrôle et sont résolues par l'algorithme SIMPLE. Les nombres de Rayleigh considérés couvrent la gamme de températures rencontrée en pratique. Une analyse détaillée de l'interaction entre les trois modes de transfert de chaleur est présentée.

Abstract
The aim of this paper is to study numerically the coupling between the heat transfers by conduction, natural convection and radiation in two-dimensional honeycomb structures. Application is presented for building honeycomb walls formed by hollow clay tiles with three or four vertical ranges of air cells. The outside and inside vertical surfaces of the studied structures are assumed to be isothermal. The upper and lower boundaries are considered to be adiabatic or submitted to a periodic condition. Equations governing conservation of mass, momentum and energy in the cavities as well as the heat conduction equation in solid walls are discretized using the control volume approach and solved using the SIMPLE algorithm. The range of Rayleigh numbers considered covers the temperature differences that occur in practice. A detailed analysis of the interaction between the three mechanisms of heat transfer is presented.

1. INTRODUCTION

Honeycomb structures are used in many applications such as thermal insulation systems or building cellular walls. Such structures generally contain a set of air-cells where the main mechanisms of heat transfer are natural convection and radiation. Overall conductances are traditionally used to describe combined convection and radiation heat transfer in air-cells especially in cases where the calculation domain is large [1,2]. However, this procedure does not give accurate results because the air temperature in the cavities is not uniform and the overall conductance value is not constant and depends on the temperature at the cells surfaces. Therefore, accurate prediction of heat transfer through honeycomb structures requires a detailed model to describe the coupled conduction, convection and radiation heat transfers. Most of the available works dealing with interactions between the three mechanisms of heat transfer are limited to the study of the effects of conduction and/or radiation on natural convection in simple cases consisting of rectangular cavities with one or several

Received 6 October 2004
Revised 4 October 2005

conducting walls. One of the first investigations was conducted by Larson and Viskanta [3]. They studied the laminar natural convection in a two-dimensional enclosure surrounded by one-dimensional conducting and radiating walls. Koutsoheras and Charters [4] performed a numerical solution of natural convection in an inclined air-cell with a finite side wall**.** Balvanz and Kuehn [5] and Lauriat [6] examined the effects of radiation on natural convection in vertical cavities including the conductive heat transfer in one of the four walls of the cavity. Numerical and experimental results for buoyancy-induced flow in a square cavity with four conducting walls were carried out by Kim and Viskanta [7]. They showed that natural convection heat transfer is markedly reduced by conduction in the walls and/or radiation exchange among the cavity surfaces. Effects of radiation on natural convection in enclosures have been studied in works of Balaji and Vankateshan [8], Akiyama and Chong [9] and Ramesh, Balaji and Vankateshan [10]. Numerical simulation of coupled heat transfers by conduction, radiation and natural convection in hollow structure with two vertical series of square air cells has been performed by Abdelbaki and Zrikem [11]. Based on results of this study, Abdelbaki et al. [12] developed a two step procedure for modeling transient heat transfer through hollow clay tiles used in building walls and determining appropriate transfer function coefficients that cannot be generated using traditional algorithms of Stephenson and Mitatas [13], Ceylan and Myers [14] and Seem [15]. In the first step of the previous study, numerical simulation of coupled heat transfers had been carried out for realistic thermal excitations. In the second step, simulation results was used to determinate the empirical transfer function coefficients by applying an identification technique.
However, hollow structures with two air-cells deep have very limited practical utilization. For example, in building construction, such components are used only in internal walls separating the rooms. The hollow clay tiles used to construct building envelopes are generally formed by three or four air-cells deep. This paper presents detailed numerical study of coupled heat transfers in more general case where honeycomb structures are formed by several air-cells in both horizontal and vertical directions. Detailed numerical simulation of coupled heat transfers in such situation requires more computational effort because the total number of cavities is important (about 64 cavities in a 72cm high honeycomb wall) and the equations governing the coupling between the three modes of heat transfer in all cavities must be solved simultaneously. The models used to predict conduction, natural convection and radiation heat transfers are described. The results are presented for cellular walls used in building envelope. Analysis of the thermal behavior of the entire system is presented. Interaction between heat conduction, natural convection and radiation is discussed. Effect of the number of air cells in the two directions of heat transfer is studied.

2. MATHEMATICAL MODEL

A schematic diagram of a honeycomb structure of aspect ratio Ar= H/L with Nx air cells deep is shown in figure 1. This structure contains Nx×Ny rectangular cavities of width l and high h surrounded by solid walls. The outside and inside vertical surfaces are assumed to be isothermal but at different temperatures T_o and T_i. The upper and lower horizontal surfaces of the structure are adiabatic or submitted to a periodic boundary condition (the temperature and heat flux in the upper boundary of the configuration are considered equal to the ones in the lower boundary). In formulating governing equations, it is assumed that the heat transfer is two-dimensional and the fluid (air) motion in the cavities is laminar. The air and the solid properties are assumed to be independent of temperature except for the air density in the buoyancy term. The fluid is Newtonian, incompressible and the Boussinesq approximation is used. Viscous heat dissipation in the fluid is assumed to be negligible. The air inside the cavities is assumed to be nonparticipating and the cell surfaces are considered diffuse-gray.

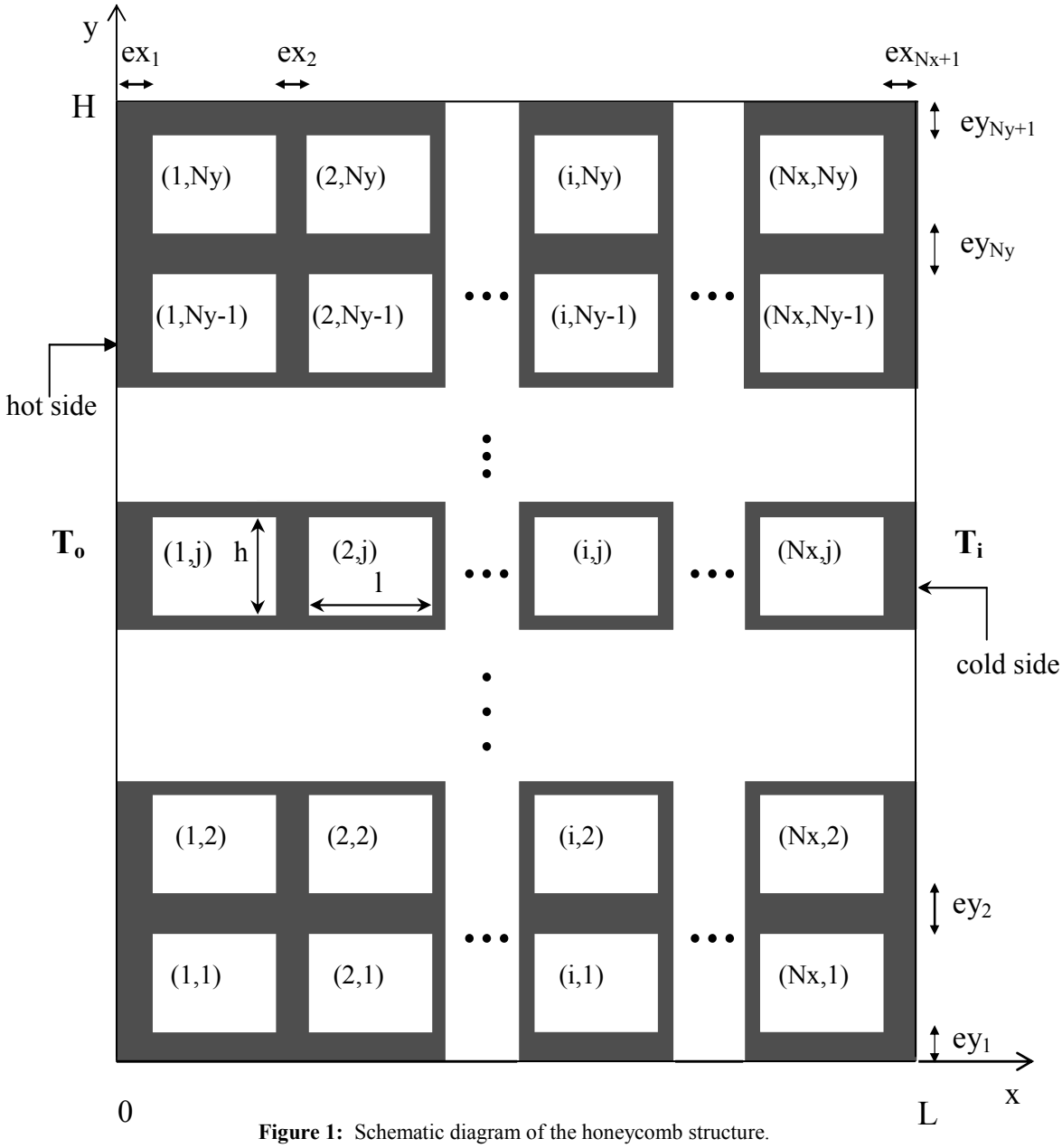

Figure 1: Schematic diagram of the honeycomb structure.

Dimensionless equations governing the conservation of mass, momentum and energy for the air in the internal cavities are given by:

$$\frac{\partial U}{\partial X} + \frac{\partial V}{\partial Y} = 0 \tag{1}$$

$$\frac{\partial U}{\partial \tau} + U\frac{\partial U}{\partial X} + V\frac{\partial U}{\partial Y} = -\frac{\partial P}{\partial X} + Pr\frac{\partial^2 U}{\partial X^2} + Pr\frac{\partial^2 U}{\partial Y^2} \tag{2}$$

$$\frac{\partial V}{\partial \tau} + U\frac{\partial V}{\partial X} + V\frac{\partial V}{\partial Y} = -\frac{\partial P}{\partial Y} + Pr\frac{\partial^2 V}{\partial X^2} + Pr\frac{\partial^2 V}{\partial Y^2} + Pr\,Ra\theta_f \tag{3}$$

$$\frac{\partial \theta_f}{\partial \tau} + U\frac{\partial \theta_f}{\partial X} + V\frac{\partial \theta_f}{\partial Y} = \frac{\partial^2 \theta_f}{\partial X^2} + \frac{\partial^2 \theta_f}{\partial Y^2} \tag{4}$$

where U and V are the velocity components in X and Y directions respectively, P is the pressure, θ_f is the fluid temperature, τ is the dimensionless time, Pr is the Prandlt number and Ra is the Rayleigh number given by:

$$Ra = \frac{g\beta L^3 (T_o - T_i)}{\nu^2} Pr$$

where g is the gravity acceleration , β is the thermal expansion coefficient and ν is the fluid kinematic viscosity. The dimensionless equation of heat conduction in the solid walls is:

$$\frac{\alpha_f}{\alpha_s}\frac{\partial \theta_s}{\partial \tau} = \frac{\partial^2 \theta_s}{\partial X^2} + \frac{\partial^2 \theta_s}{\partial Y^2} \tag{5}$$

where α_f and α_s are the fluid and the solid thermal diffusivities respectively and θ_s is the dimensionless solid temperature. The boundary conditions of the problem are:

- U= V= 0 on the cavities surfaces
- $\theta_s(0,Y)= 1$ and $\theta_s(1,Y)= 0$ $(0 \le Y \le Ar)$

$$\left.\frac{\partial \theta_s}{\partial Y}\right)_{Y=0} = \left.\frac{\partial \theta_s}{\partial Y}\right)_{Y=Ar} = 0 \qquad 0 \le X \le 1 \qquad \text{for the adiabatic condition}$$

- or

$$\theta_s(X,0) = \theta_s(X,Ar) \qquad 0 \le X \le 1 \qquad \text{for the periodic condition}$$

The continuity of the temperature and the heat flux at the fluid-wall interfaces gives:

$$\theta_s(X,Y)= \theta_f(X,Y) \tag{6}$$

$$-\frac{\partial \theta_s}{\partial \eta} = -N_k\frac{\partial \theta_f}{\partial \eta} + N_r Q_r \tag{7}$$

where η represents the dimensionless coordinate normal to the wall, N_k is the ratio of the solid thermal conductivity k_s to the fluid one k_f ($N_k=k_s/k_f$), Qr is the dimensionless net radiative heat flux and N_r is the dimensionless radiation to conduction parameter defined by:

$$N_r = \frac{\sigma T_o^4 L}{k_s (T_o - T_i)}$$

σ is the Stefan-Boltzman constant. The dimensionless radiative heat flux Qr is related to non-dimensionless one qr by

$$Qr = \frac{qr}{\sigma T_o{}^4}$$

The net radiative heat flux $q_{rk}(r_k)$ exchanged by the finite area dA_k located at a position r_k on surface k is given by [16]:

$$qr_k(r_k) = J_k(r_k) - E_k(r_k) \tag{8}$$

where $J_k(r_k)$ is the radiosity and $E_k(r_k)$ is the incident radiative heat flux on surface dA_k given respectively by:

$$J_k(r_k) = \varepsilon_k \sigma (T_k(r_k))^4 + (1-\varepsilon_k) E_k(r_k) \tag{9}$$

$$E_k(r_k) = \sum_{j=1}^{4} \int_{A_j} J_j(r_j) dF_{dA_k - dA_j}(r_k, r_j) \tag{10}$$

where ε_k is the emissivity of the surface k and $dF_{dA_k - dA_j}$ is the view factor between the finite surfaces dA_k and dA_j located at r_k and r_j respectively. Taking into account equations (8), (9) and (10), the dimensionless radiative heat flux can be expressed as

$$Qr_k(r_k') = \varepsilon_k (1-\frac{1}{G})^4 \left[\theta_k(r_k') + \frac{1}{G-1} \right]^4 - \varepsilon_k \sum_{j=1}^{4} \int_{A_j} J_j'(r_j') dF_{dA_k - dA_j} \tag{11}$$

where G is the ratio of the temperatures of the honeycomb structure surfaces ($G=T_o/T_i$), $J'_j(r'_j)$ is the dimensionless radiosity at the position r'_j on surface j. By dividing each cavity surface into finite isothermal area, equation (11) leads to a set of linear equations where the unknowns are the dimensionless radiosities $J'_j(r'_j)$.
The local Nusselt number at a cavity side is defined as:

$$Nu = \frac{h_{conv} L}{k_f} = -\left. \frac{\partial \theta_f}{\partial \eta} \right|_{surface} \tag{12}$$

where h_{conv} is the natural convection coefficient given by:

$$h_{conv} = -\frac{k_f \left. \frac{\partial T_f}{\partial \xi} \right|_{surface}}{(T_o - T_i)} \tag{13}$$

ξ represents the coordinate normal to the cavity surface (η=ξ/L).
The dimensionless average heat flux at the vertical wall surfaces is given by:

$$\overline{Q} = -\frac{1}{Ar}\int_0^{Ar}\left(\frac{\partial\theta}{\partial X}\right)_{X=0} dY \tag{15}$$

The transient equations given previously are solved to obtain steady-state solution using the control volume approach and the SIMPLE algorithm. The resulting system of algebraic equations is solved using a line-by-line method. The integration on time is fully implicit. A study on the effects of both grid spacing and time step on the simulation results has been conducted. The compromise between accuracy and computational time is found for the non-uniform grids given in table 1.

Nx×Ny	4×16	4×8	4×4	4×1	3×16	3×8	3×4	3×1
grid	103×403	103×203	103×103	103×28	78×403	78×203	78×103	78×28

Table 1: Grids used for the different processed configurations.

A 22×22 non-uniform grid is used in each cavity. The differences obtained, in the overall heat flux, using 30×30 non-uniform grid are lower than 0,1% for $Ra=10^6$ and than 0,5% for $Ra=10^8$. The dimensionless time used in the simulation is 10^{-4}. The convergence criterion is based on the relative changes in the variables U,V,P, θ and Qr at the different nodes of the calculation domain:

$$\left|\frac{f^{n+1}(i,j) - f^{n}(i,j)}{f^{n}(i,j)}\right| \le 10^{-5}$$

where $f^n(i,j)$ is the value of the variable f (f= U, V, P, θ or Qr) at node (i,j) calculated in the iteration n. The numerical code was tested [11] by comparing its results with those obtained by De Vahl Davis [17] and Le Breton et al. [18] in the case of natural convection in a differentially heated cavity. The code was also tested in the case of interaction between natural convection and radiation in a square cavity by comparing its results with those obtained in studies [8,9,10]. The comparison showed that there is a good agreement between the results of the present code and the previous studies results.

3. RESULTS

Results presented in this study have been obtained for cellular walls made of hollow clay tiles formed by square cavities with h= l= 3.5cm separated by 1cm thick clay slabs (ex_i= ey_j= 1cm for $1\le i \le Nx+1$ and $2\le j \le Ny$). The lower and upper horizontal walls are 0.5cm thick (ey_1= ey_{Ny+1}= 0.5cm). These dimensions are those used to make practical hollow clay tiles. The cellular wall aspect ratio Ar depends upon the numbers of cells in x and y directions. Then for a wall with four air cells deep (Nx= 4) the aspect ratio values corresponding to Ny= 1, 4, 8 and 16 are 0.24, 0.95, 1.89 and 3.79 respectively. The other parameters used in the simulation are N_k = 0.025, Pr= 0.71 and ε_i= 0.8. The Rayleigh number ranges from 5.10^5 to 2.10^7 for Nx= 3 and from 5.10^5 to 4.10^7 for Nx= 4. This corresponds to a temperature difference $\Delta T=(T_o-T_i)$ between 0.5 and 70°C. This range widely covers the temperature differences that occur in practice.

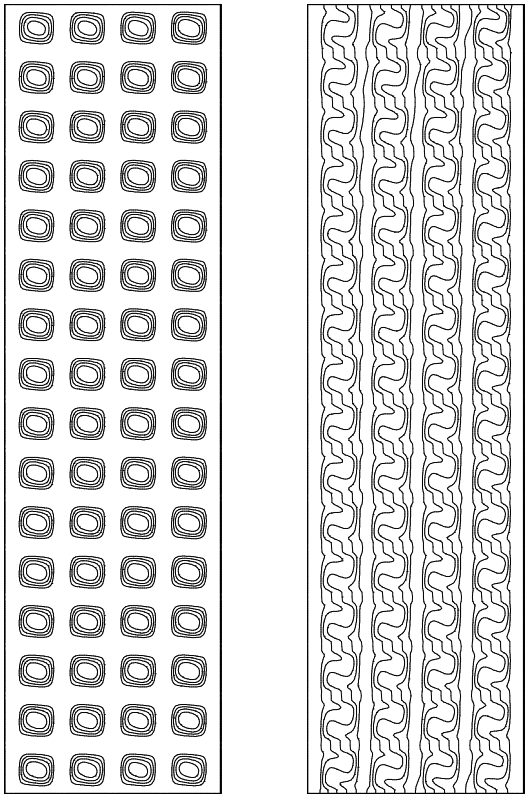

Figure 2: Streamlines (a) and isotherms (b) obtained for *Nx*= 4, *Ny*= 16, *Ra*= 2.53 10^7, *G*= 1.14 and *Nr*= 3.27.

3.1. Streamlines and isotherms

For Ra= 2.53.10^7 , Nr= 3.27, G= 1.14, Nx= 4 and Ny= 16, figures 2.a and 2.b illustrate the contours of the streamlines and the isotherms respectively obtained for adiabatic wall horizontal surfaces. It appears from figure 2.a that the flow field has the same form in all cavities and is characterized by a single cell circulating clock-wise. Comparison of the flow structures in each horizontal row of cavities shows that the size of the central streamline increases slightly from the left cavity (*i*=1) to the right one (*i*= 4) indicating an increase in the flow intensity. This increase is about 2.5% and is attributed to the diminishing effect of the radiation on natural convection in the right cavities. Results of figure 2.b show that the temperature profile is almost linear near the centerline of the horizontal walls separating the cavities where the isotherms are spaced almost equally. However, there exists a weak vertical heat transfer across the horizontal walls. Thus, the linear behavior is not perfect and is violated in the cavities because of the natural convection heat flow. Therefore, the temperature gradient in each cavity becomes more important near both the lower part of the left vertical side and the upper part of the right vertical one than in the rest of the cavity. Note that the flow structures and isotherms obtained when considering other values of *Ny* and/or imposing periodic boundary conditions to the upper and lower wall horizontal surfaces are similar to those presented in figure 2.

3.2. Local Nusselt number

Since there are 64 cells in the studied structure, analysis cannot be presented for all cells and only representative series of cavities are considered. For the 8th horizontal row, figure 3 illustrates the variations of the local Nusselt number along the vertical walls as a function of the dimensionless vertical position from the cavity lower side Y'. Results show that the local Nusselt number at the left vertical side (hot side) attains its highest value in the lower half of the cavity (near Y'= 0.05) while the maximum in convection heat transfer at the right vertical side (cold side) occurs in the upper half of the cavity (near Y'= 0.14). These results are compatible with those reported in the literature [7,19]. As it has been observed for the flow intensity (figure 2.a), the increase in local Nusselt number from the left cavity (i=1) to the right one (i= 4) is due essentially to the interaction between radiation and convection heat transfers. In fact, the radiation heat exchange is more important in the left cavities and its effect on natural convection in these cavities is more pronounced. Therefore, natural convection heat transfer is more attenuated in left cavities than in right ones. Discrepancies between results obtained in the different cavities are appreciable near the maximum Nusselt number and become negligible in the vicinity of the corners.

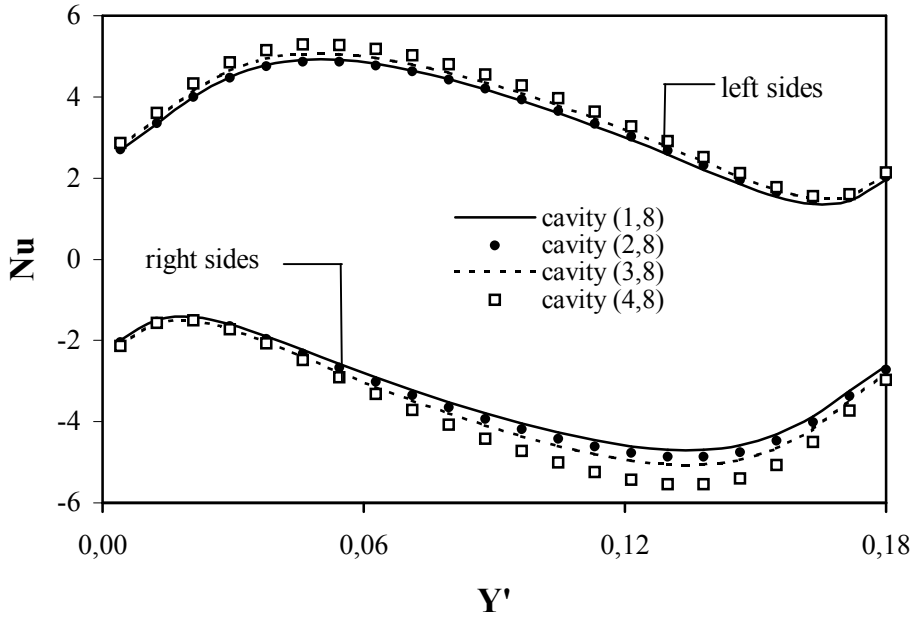

Figure 3: Variation of the local Nusselt number along the vertical surfaces.

3.3. Local net radiative heat flux

For the cavities of the 8th row the variations of the local dimensionless net radiative heat flux along the vertical and horizontal walls are illustrated in figure 4. As it can be seen, for each cavity, the radiative heat flux leaving the left vertical wall (or received by the right one) is minimum near the corners and attains its highest value near the midpoint of the wall (Y'=0.09). The radiation heat transfer decreases considerably from the left cavity (i=1) to the right one (i=4). In fact the difference between the two cavities exceeds at some points 20%. This is due essentially to the important decrease in temperature which vari, for example, from 0.98 at the midpoint of the left vertical wall in the cavity (1,8) to 0.26 in the cavity (4,8).

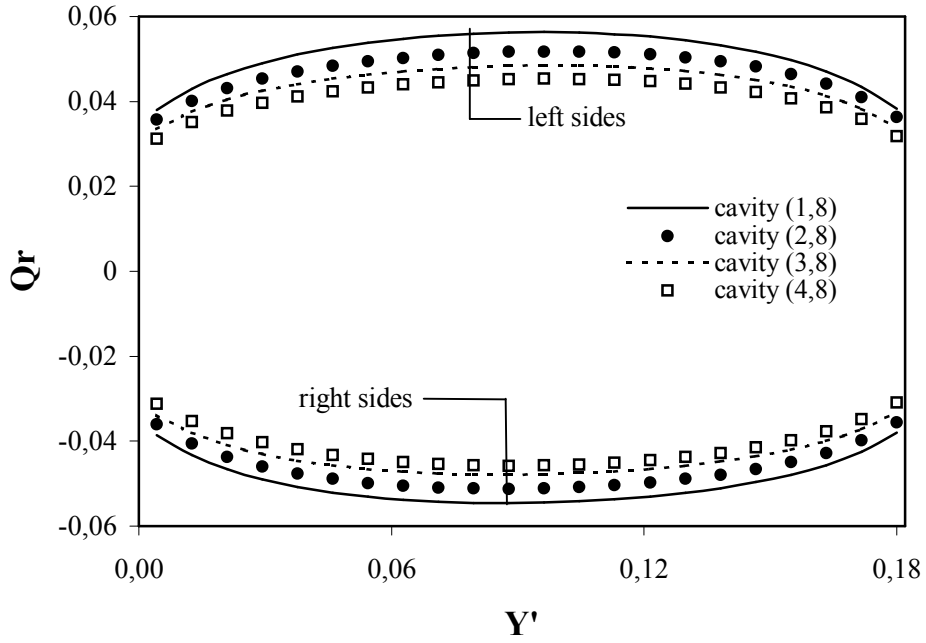

Figure 4: Variation of the dimensionless radiative heat flux along the vertical surfaces.

3.4. Variations of Nusselt number and radiative heat flux in a vertical range

In order to compare heat transfer by convection or by radiation in cells of a vertical series (y direction), figures 5 and 6 give the variations of local Nusselt number and dimensionless radiative heat flux respectively along the vertical walls of some cavities of the first vertical range (i=1). As it can be seen, the results obtained in the different cells are similar except for the cavities neighboring the upper and lower boundaries where the results obtained differ appreciably from those predicted in the other cavities. In fact , the maximum difference between the results obtained in the cavities (1,4), (1,8) and (1,12) does not exceed 1.8% for the radiative heat flux and 1.6% for the local Nusselt number. However the difference in radiative heat flux reaches at some points 8% between the cavities (1,1) and (1,4) on one hand and 9% between the cavities (1,12) and (1,16) on the other hand. These differences exceed 10% for the local Nusselt number. This is due essentially to the edge effects that result from the zero heat flux condition imposed at both the upper and the lower structure boundaries. In fact, because of the rising vertical heat transfer across the horizontal walls separating the cavities, all cells are heated from below and cooled from above except for the cavities (1,1) and (1,16) for which the top wall and the bottom one respectively are assumed to be adiabatic. The rising vertical heat transfer is caused by natural convection that creates a temperature gradient between the upper and lower surfaces of each separating wall. The underside of the latter is heated by the hot fluid flowing from the left corner to the right one while its top side is cooled by the cold fluid circulating in the opposite direction. Therefore the heat leaving the lower cell (j=1) to the next one (j=2) is not compensated for and the temperature gradient becomes more important in this cell. So, the Nusselt number and the radiative heat flux are greater than those in the other cavities. On the contrary, the heat coming to the upper cell (j= 16) from below does not leave it and tends to homogenize the temperature field in the upper part of the studied structure. This explains the fact that Nusselt number and radiative heat flux in the cavity (1,16) are lower than those obtained in the other cells.

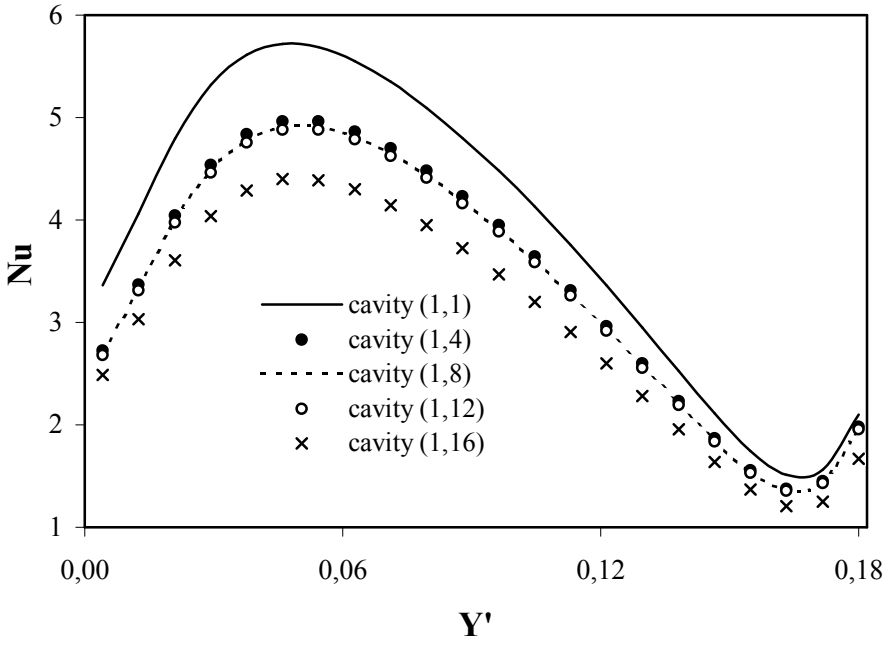

Figure 5: Variation of the local Nusselt number at the left vertical side of the first vertical cells range.

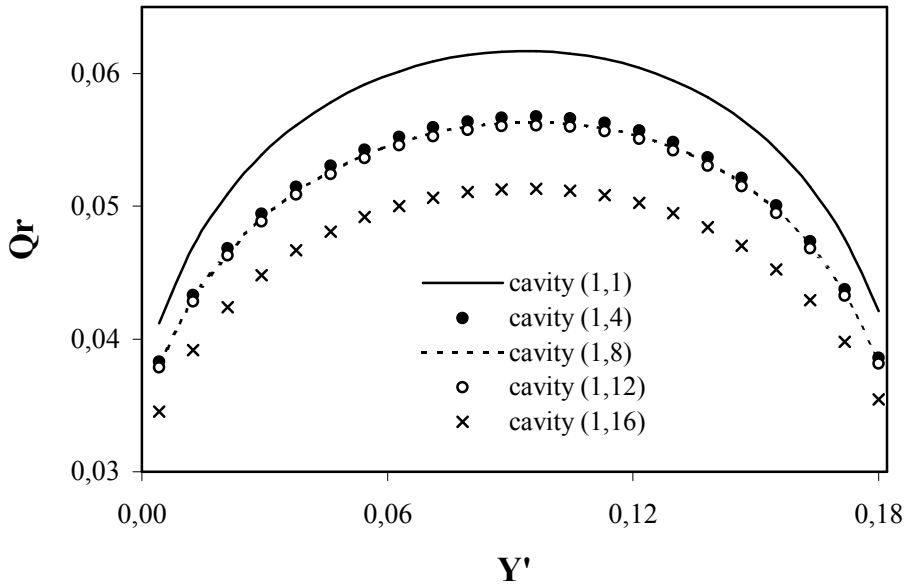

Figure 6: Variation of the dimensionless radiative heat flux along the left vertical side of the first vertical cells range.

3.6. Effects of both Ny value and horizontal boundaries condition

The two kinds of boundary conditions envisaged for the upper and lower configuration surfaces are based on physical considerations. In fact, if the adiabatic boundary condition is attributed to the fact that mean lateral heat flux remains negligible compared to the horizontal one, the periodic boundary condition is based on the geometric periodicity of the configuration under investigation. However, it is necessary to determinate the system optimum height to be considered to obtain sufficiently accurate results without enough perturbing the thermal behavior of this system. The height of the system is determined by the number of cells in vertical direction (Ny).

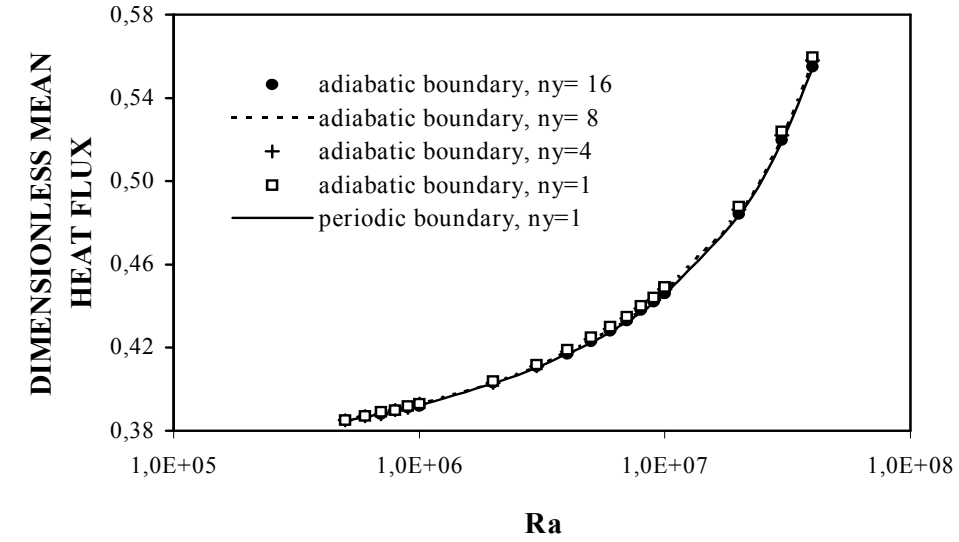

(a)

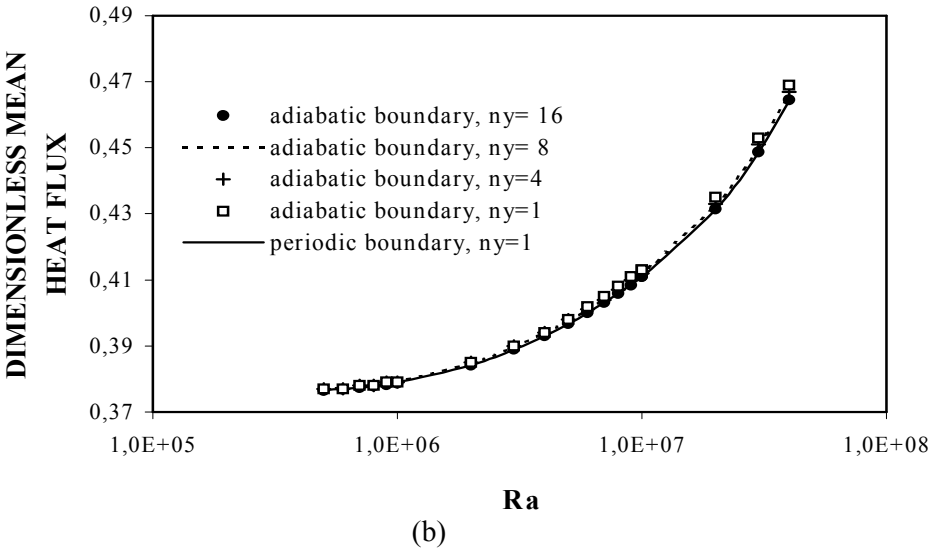

(b)

Figure 7: Effects of both *Ny* and horizontal boundaries condition on the heat flow through the cellular wall : (a) *Nx*= 3 ; (b) *Nx*= 4.

Figure 7 gives the variations of the mean dimensionless heat flux ($\overline{Q}$) at the wall hot/cold side against the Rayleigh number for different values of Ny. The two types of horizontal boundary conditions (adiabatic and periodic boundary conditions) are used. It can be seen that results obtained in all cases are similar. The differences between these results do not exceed 1% for both Nx=3 and Nx=4. The heat fluxes obtained when the upper and lower configuration boundaries are insulated tend towards those predicted using periodic boundary condition as Ny increases. In fact, as it had been see in the previous sections edge effects caused by adiabatic conditions are appreciable only in regions situated near the horizontal boundaries. So, these effects are attenuated by the increase in Ny. Therefore the study of the entire system formed by Nx×Ny (Ny>1) air-cells can be reduced with a very good approximation to that of hollow block with one horizontal range of air-cells (Nx×1 hollow block). This approximation permits significant reduction in computational time especially in transient conditions where the latter becomes extremely high.

3.7. Comparison of heat transfer modes

Based on the result established above the following study is limited to Nx×1 hollow clay tile. In order to evaluate the contribution of the three heat transfer modes to the overall heat flow, dimensionless average heat fluxes by conduction, convection and radiation are defined at a cavity left side level respectively as:

$$Q_{cond} = -\frac{L}{ey_1}\int_0^{\frac{ey_1}{L}} \frac{\partial \theta_S}{\partial X}\Bigg)_{X'=0} dY - \frac{L}{ey_2}\int_{\frac{(h+ey_1)}{L}}^{\frac{H}{L}} \frac{\partial \theta_S}{\partial X}\Bigg)_{X'=0} dY \tag{17}$$

$$Q_{conv} = -\frac{L}{h} N_k \int_{\frac{ey_1}{L}}^{\frac{(h+ey_1)}{L}} \frac{\partial \theta_f}{\partial X}\Bigg)_{X'=0} dY \tag{18}$$

$$Q_{rad} = +\frac{L}{h} N_r \int_{\frac{ey_1}{L}}^{\frac{(h+ey_1)}{L}} Q_r(Y)\, dY \tag{19}$$

The values of these fluxes are calculated for *Nx*= 4 over a range of Rayleigh numbers at the level of first cavity left side and are presented in terms of percentages in figure 8. The results of this figure indicate that heat conduction is predominant because it represents more than 50% of the overall heat transfer. However, the contributions of both convection and radiation heat transfers are not negligible and increase at the detriment of conduction as the Rayleigh number increases. The heat transfer by radiation is almost twice greater than that by convection. It should be noted that these results do not significantly change in the other cavities.

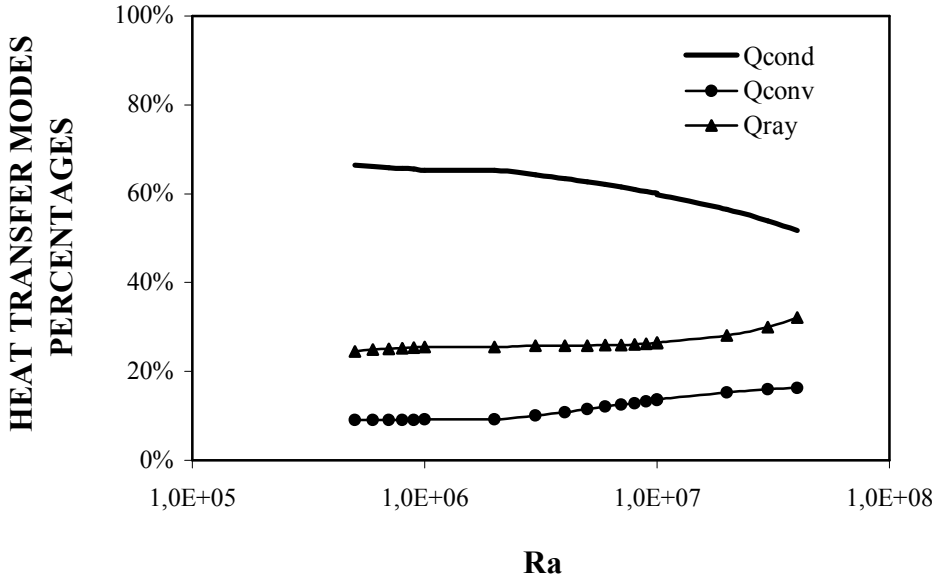

Figure 8: Contribution of different heat transfer modes to the overall heat flow through the honeycomb wall.

4. CONCLUSION

The results of this study showed that radiation heat transfer decreases considerably from the left cavity of horizontal range of cells to the right one. This is due essentially to the important decrease in temperature. Consequently, natural convection heat transfer is more attenuated by radiation heat exchanges in left cavities. However, results obtained in the cells of a vertical series concerning local Nusselt number, radiative heat flux and lateral heat transfer are similar except for the cavities neighboring the upper and lower adiabatic boundaries where the results obtained differ appreciably from those predicted in the other cavities. Also, it had been shown that it is possible to reduce the study of the entire system to that of hollow block with one horizontal range of air-cells. This approximation permits significant reduction in computational time especially in the case of transient thermal excitations

5. REFERENCES

1. Ashrae Handbook of Fundamentals. Atlanta GA USA; (1981, 1985, 1989).
2. Balvanz J. L., Kuehn T. H., Effect of wall conduction and radiation on natural convection in a vertical slot with uniform heat generation on the heated wall, ASME HTD; Vol. 8, pp. 55-62, (1980).
3. EL Biyaâli A., Roux J. J., Yezou R., Ayaichia H., Application de la réduction de modèles aux singularités thermiques de bâtiments, Revue Générale de Thermique, N° 394, pp. 571-579, (1994).
4. Koutsoheras W., Charters W. W. S., Natural convection phenomena in inclined cells with finite side-walls: a numerical solution, Energy, Vol.19, pp. 433-438, (1977).
5. Larson D. W., Viskanta R., Transient combined laminar free convection and radiation in a rectangular enclosure, J. Fluid Mech., pp.78: 65-85, (1976).

6. Lauriat G., A numerical study of a thermal insulation enclosure: influence of the radiative heat transfer, ASME HTD; Vol. 8, pp. 63-71, (1980).
7. Kim D.M., Viskanta R., Effect of wall conduction and radiation on natural convection in a rectangular cavity, Num. Heat Transfer; Vol. 7, pp. 449-470, (1984).
8. Balaji C., Venkateshan S. P., Correlations for free convection and surface radiation in a square cavity, Int. J. Heat Fluid Flow, Vol. 15, pp. 249-251, (1994).
9. Akiyama M., Chong Q. P., Numerical analysis of natural convection with surface radiation in a square enclosure, Num. Heat Transfer, Vol. 31, Part A, pp. 419-433, (1997).
10. Ramesh N., Balaji C., Venkateshan S. P., Effects of boundary conditions on natural convection in enclosures, Int. J. Transport Phenomena, Vol. 1, pp. 205-214, (1999).
11. Abdelbaki A., Zrikem Z., Simulation numérique des transferts thermiques couplés à travers les parois alvéolaires des bâtiments, Int. J. Therm. Sc., Vol. 38, pp. 719-730, (1999).
12. Abdelbaki A., Zrikem Z., Haghighat F., Identification of empirical transfer function coeffients for a hollow tile based on detailed models of coupled heat transfers, Building and Environment , Vol. 36, pp. 139-148, (2001).
13. Stephonson D. G., Mitalas G. P., Calculation of heat conduction transfer functions for multi-layer slabs, Ashrae Trans., Vol 77, Part II, pp. 117-126, (1971).
14. Ceylan H.T., Myers G.E., Long-time solutions to heat conduction transient with time-dependent inputs, ASME J. Heat Transfer, Vol. 102, pp. 115-120, (1980).
15. Seem J.E., Modeling in heat transfer in buildings, Ph. D. thesis. Madison: University of Wisconsin; (1987).
16. Siegel R., Howell J. R., Thermal radiation heat transfer, 2d ed. New York: McGraw-Hill; (1981).
17. De Vahl Davis G., Natural convection of air in a square cavity: a Bench Mark numerical solution, Int. J. Num. Meth. Fluids, Vol. 3, pp. 249-264, (1983).
18. Le Breton P., Caltagirone J.P., Arquis E., Natural convection in square cavity with thin porous layers on its vertical walls, ASME J. Heat Transfer, Vol. 113, pp. 892-898, (1991).
19. Bajorek S.M., Lloyd J.R., Experimental investigation of natural convection in partitioned enclosures, ASME J. Heat transfer, Vol. 104, pp. 527-532, (1982).